

PAPER



Cite this: *Phys. Chem. Chem. Phys.*,
2019, 21, 1578

Uncovering the role of the stationary points in the dynamics of the $F^- + CH_3I$ reaction†

Balázs Olasz and Gábor Czakó *

We describe an analysis method which assigns geometries to stationary points along (quasi)classical trajectories. The method is applied to the $F^- + CH_3I$ reaction, thereby uncovering the role of the minima and transition states in the dynamics of the S_N2 inversion, S_N2 retention *via* front-side attack and double inversion, induced inversion, and proton-transfer channels. Stationary-point probability distributions, stationary-point-specific trajectory orthogonal projections, root-mean-square distance distributions, transition probability matrices, and time evolutions of the stationary points reveal long-lived front-side ($F^- \cdots ICH_3$) and hydrogen-bonded ($F^- \cdots HCH_2I$) complexes in the entrance channel and significant post-reaction ion-dipole complex ($FCH_3 \cdots I^-$) formation in the S_N2 exit channel. Most of the proton-transfer stationary points ($FH \cdots CH_2I^-$) participate in all the reaction channels with larger distance deviations than the double-inversion transition state. Significant forward–backward transitions are observed between the minima and transition states indicating complex, indirect dynamics. The utility of distance and energy constraints is also investigated, thereby restricting the assignment into uniform configuration or energy ranges around the stationary points.

Received 5th October 2018,
Accepted 20th December 2018

DOI: 10.1039/c8cp06207b

rsc.li/pccp

I. Introduction

Mechanisms of chemical reactions are usually depicted by interconnected stationary-point structures. These stationary points can be minima (complexes or intermediates) or saddle points (transition states) on the potential energy surface (PES) of the chemical system. Because there are only a finite number of stationary points among the infinite number of nuclear configurations, in a mathematical point of view, the probability of going exactly through a stationary point is zero. Nevertheless, many chemical reactions “approach” the stationary points along their reaction pathways as classical dynamics simulations show. Of course, exemptions also exist, for example, the $OH^- + CH_3F$ reaction avoids the deep minimum in the exit channel.¹ The above statements are based on human inspection of trajectory animations while the role of the stationary points is qualitatively determined. Here, following some previous work,^{2–9} we report a quantitative analysis technique that numerically assigns each configuration along classical

trajectories to a stationary point of the PES. Then, we can compute the probability distributions of the assigned minima and transition states, we can quantify the “approach” of a stationary point, and we can track transitions between stationary points. We apply the analysis method to the $F^- + CH_3I$ reaction, because this system is under current experimental and theoretical investigations,^{10–20} but the role of the stationary points in the dynamics is still not fully clear. Many stationary points have already been characterized^{10,11,13–15} and in 2017 we developed a global *ab initio* analytical PES which describes the Walden-inversion, front-side attack retention, double-inversion (retention) pathways as well as the proton-transfer channel.¹⁴ Later in 2017 direct dynamics simulations of Hase and co-workers¹⁵ confirmed our previously proposed double-inversion pathway *via* a so-called double-inversion transition state. However, it was also shown that double inversion is a non-intrinsic-reaction-coordinate (non-IRC) pathway, whereas IRC computations connect the double-inversion transition state to the proton-transfer channel.^{13,15} One of the goals of the present study is to uncover the role of the double-inversion and proton-transfer stationary points in the dynamics of the $F^- + CH_3I$ reaction by numerically analyzing millions of trajectories. In Section II we give the details of our methodology and trajectory computations. Furthermore, the relation of the present stationary-point assignment approach to previous work is also described in Section II. The results are presented and discussed in Section III and the paper ends with summary and conclusions in Section IV.

Interdisciplinary Excellence Centre and Department of Physical Chemistry and Materials Science, Institute of Chemistry, University of Szeged, Rerrich Béla tér 1, Szeged H-6720, Hungary. E-mail: gczako@chem.u-szeged.hu

† Electronic supplementary information (ESI) available: Definition of the interaction region and detailed results (stationary-point probabilities with and without distance and energy constraints, trajectory orthogonal projections, RMS distance distributions, and transition probability matrices) at seven different collision energies as well as stationary points as a function of time for selected trajectories. See DOI: 10.1039/c8cp06207b

II. Methods and computational details

Each actual geometry, whose Cartesian coordinates are \mathbf{r} , along a trajectory is assigned to one of the stationary points, whose center of mass Cartesian coordinates are $(\mathbf{r}^{\text{stat}})_k$, as follows. Let us move \mathbf{r} into the center of mass frame and compute:^{6,21}

$$(A_{n,m})_k = \sum_{i=1}^N m_i r_{i,n} (r_{i,m}^{\text{stat}})_k \quad n, m = 1(x), 2(y), 3(z), \quad (1)$$

$$(\mathbf{A}_1)_k = (\mathbf{A}^T)_k \mathbf{A}_k \text{ and } (\mathbf{A}_2)_k = \mathbf{A}_k (\mathbf{A}^T)_k, \quad (2)$$

$$\mathbf{C}_k = (\mathbf{U}_1)_k (\mathbf{U}_2^T)_k, \quad (3)$$

where N is the number of atoms, m_i ($i = 1, 2, \dots, N$) denotes the masses, $k = 1, 2, \dots, N_{\text{stat}}$, where N_{stat} is the total number of stationary points, and the columns of \mathbf{U}_1 and \mathbf{U}_2 contain the normalized eigenvectors of the real symmetric matrices \mathbf{A}_1 and \mathbf{A}_2 , respectively. The best overlap in mass-scaled Cartesian coordinates between the actual geometry and $(\mathbf{r}^{\text{stat}})_k$ is obtained as $\mathbf{C}_k \mathbf{r}$, which is equivalent with satisfying the Eckart conditions.²² The stationary point is assigned to \mathbf{r} by minimizing

$$\text{RMS}(k) = \sqrt{\sum_{i=1}^N \sum_{n=1}^3 \left((\mathbf{C}_k \mathbf{r})_{i,n} - (r_{i,n}^{\text{stat}})_k \right)^2 / N}, \quad (4)$$

$$k = 1, 2, \dots, N_{\text{stat}},$$

with respect to k . Due to the fact that the relative signs of the eigenvectors stored in \mathbf{U}_1 and \mathbf{U}_2 are not well defined, eight different \mathbf{C}_k matrices can be constructed *via* eqn (3), we use the one which gives the smallest $\text{RMS}(k)$. Furthermore, $\text{RMS}(k)$ depends on the numbering of the identical atoms in \mathbf{r} relative to $(\mathbf{r}^{\text{stat}})_k$. Therefore, in general, one needs to consider all the permutations of the identical atoms when minimizing $\text{RMS}(k)$. In the case of the present application for the $\text{F}^- + \text{CH}_3\text{I}$ system, six H-atom permutations exist, providing the same $\text{RMS}(k)$ values for C_{3v} stationary points and 3 different $\text{RMS}(k)$ for the C_s references after minimizing with respect to the above-mentioned 8 \mathbf{C}_k matrices. Note that 4 \mathbf{C}_k matrices describe pure rotations, whereas the other 4 matrices correspond to pseudo-rotation (rotation + inversion) taking care of chirality problems.

At this point we note some previous work related to the above-described approach. In 1984 Stillinger and Weber² proposed a steepest descent method to relax a non-stationary structure of a liquid or solid into a minimum of the PES. In 2009 we also used similar geometry optimization method for polyatomic quasiclassical mode-specific product analysis.³ If the equilibrium structure(s) of the system is(are) known a priori, one can relate the actual configuration to a minimum structure by finding the best overlap between the coordinates as Espinosa-García⁷ and others⁸ did for polyatomic product analysis of reactions and we did for analyzing the dynamics of small water clusters.^{4,5} In 2012 one of the present authors⁶ implemented an Eckart-transformation method for mode-specific polyatomic product analysis, which was used for several atom + methane²³ and S_N2 reactions²⁴ and played an important role in the discovery of the double-inversion mechanism²⁵ of S_N2 reactions. In the

present study we extend this Eckart product analysis methodology to assign any configuration along trajectories to any reference structure, which can be a stationary point as in the case of this work. Finally we note that the goal of our Eckart-transformation-based approach is similar to that of Taketsugu and co-workers,⁹ who recently assigned trajectory geometries to IRC points using a minimum-distance method *via* the Kabsch algorithm.²⁶

We perform quasiclassical trajectory computations for the $\text{F}^- + \text{CH}_3\text{I}$ reaction using our full-dimensional *ab initio* analytical PES.¹⁴ The CH_3I reactant is prepared in vibrational ground state using standard normal mode sampling. Impact parameters (b) are scanned from 0 to b_{max} , with steps of 0.5 bohr and 5000 trajectories are computed at each b . Trajectories are run at collision energies of 1.0, 4.0, 7.4, 10.0, 15.9, 35.3, and 50.0 kcal mol⁻¹ and the corresponding b_{max} values are 30, 20, 17, 15, 13, 10, and 9 bohr, respectively. We use a time step of 0.0726 fs and record the geometries at every 10th step until the maximum of the inter-atomic distances becomes 1 bohr larger than the initial one. We assign every recorded structure, *i.e.*, hundreds of gigabytes of data, in the interaction region to one of the stationary points using the technique described above. The interaction region, which excludes the reactant and product channels, is defined based on geometrical constraints as described in detail in the ESI.†

Stationary-point probabilities are determined for each reaction channel as

$$P(k, b) = \frac{N(k, b)}{N_{\text{total}}(b)}, \quad (5)$$

where $N(k, b)$ is the number of configurations assigned to the k th stationary point at impact parameter b and $N_{\text{total}}(b)$ is the total number of configurations in the interaction region recorded for all the trajectories (nonreactive and reactive independently from the reaction channels) at a given b . Then, the average stationary-point probabilities can be obtained as

$$\langle P(k) \rangle = \int_0^{b_{\text{max}}} 2\pi b P(k, b) db / \pi b_{\text{max}}^2. \quad (6)$$

Eqn (6) can be approximated with numerical integration applying the trapezoidal rule using the $P(k, b)$ values at $b/\text{bohr} = 0.0, 0.5, 1.0, \dots, b_{\text{max}}$ as it is done in the present work.

III. Results and discussion

A. Stationary points

The stationary points of the PES of the $\text{F}^- + \text{CH}_3\text{I}$ reaction are shown in Fig. 1. Here we consider four reaction channels, S_N2 inversion, S_N2 retention *via* front-side attack (FSA) and double inversion (DI), induced inversion, and abstraction as seen in Fig. 1. S_N2 inversion presumably occurs *via* several submerged minima and transition states such as $\text{HMIN} \rightarrow \text{HTS} \rightarrow \text{PREMIN} \rightarrow \text{WALDENTS} \rightarrow \text{POSTMIN}$ leading to $\text{I}^- + \text{CH}_3\text{F}$ with inversion of the initial configuration. S_N2 retention can proceed with front-side attack *via* a high-energy transition state (FSTS) or with double inversion whose first and second inversions go *via* DITS and WALDENTS, respectively, as our previous dynamics

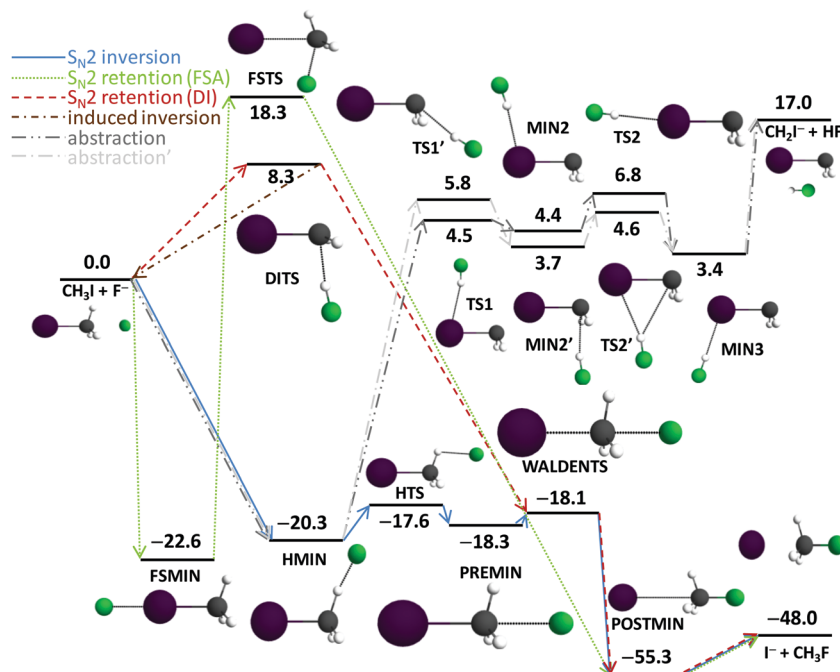


Fig. 1 Schematic potential energy surface of the $F^- + CH_3I$ reaction showing the stationary points and their classical relative energies (kcal mol^{-1}) corresponding to the analytical PES along the different reaction pathways. The figure is adapted from Fig. 1 in ref. 14.

simulations showed.^{14,25} Induced inversion results in an inverted reactant CH_3I molecule *via* DITS. Abstraction (proton transfer) may occur *via* several $FH \cdots (CH_2I^-)$ -like stationary points resulting in $HF + CH_2I^-$ products.^{13,14} Of course, the role of the above-mentioned stationary points in the dynamics of the $F^- + CH_3I$ reaction has not been fully clarified yet. Is the DITS involved in the abstraction process? Do the abstraction stationary points take part in the double-inversion mechanism? Is there any way to return from the POSTMIN region (recrossing)? What is the role of the various entrance-channel complexes in the dynamics? We seek answers for these questions utilizing the stationary-point assignment method.

B. Stationary-point probability distributions

$P(k, b=0)$ and $\langle P(k) \rangle$ values, normalized for each reaction channel of $F^- + CH_3I$, are shown in Fig. S1 (ESI[†]) for all the collision

energies and representative results at a collision energy of $35.3 \text{ kcal mol}^{-1}$ are given in Fig. 2. As Fig. 2 and Fig. S1 (ESI[†]) show front-side complex (FSMIN) formation is significant at all collision energies and available reaction channels, besides trapping in the HMIN and HTS regions. Surprisingly, the “textbook” ion-dipole complex (PREMIN) formation is almost negligible. To further investigate this somewhat unexpected finding, we project¹⁶ the position of F^- onto one of the H-C-I planes in the case of the geometries assigned to one of the FSMIN, HMIN, HTS, and PREMIN stationary points. Fig. 3 and Fig. S2 (ESI[†]) show the stationary-point-specific distributions of F^- in the entrance channel of the $F^- + CH_3I$ reaction. As seen, the distributions are spread in the front-side (iodine-side) and back-side (CH_3 -side) regions, but in the front-side region the position of F^- is more localized around the collinear FSMIN stationary-point structure,

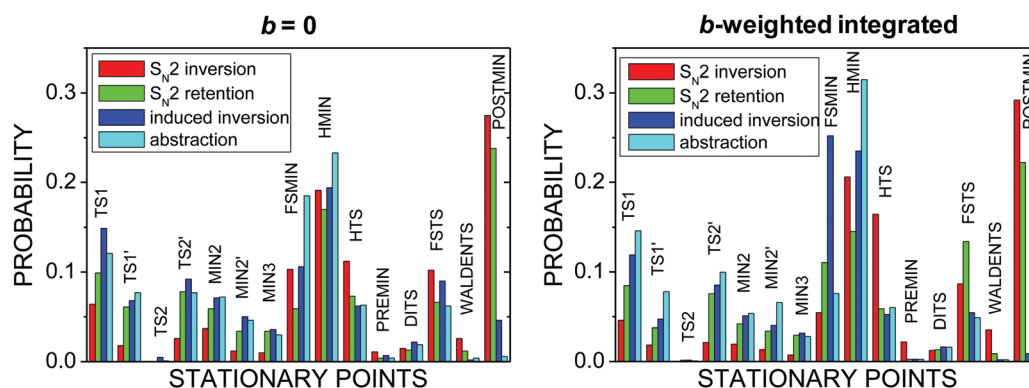


Fig. 2 Stationary-point probability distributions, normalized for each channel, corresponding to $b=0$ and b -averaged $F^- + CH_3I$ trajectories at a collision energy of $35.3 \text{ kcal mol}^{-1}$.

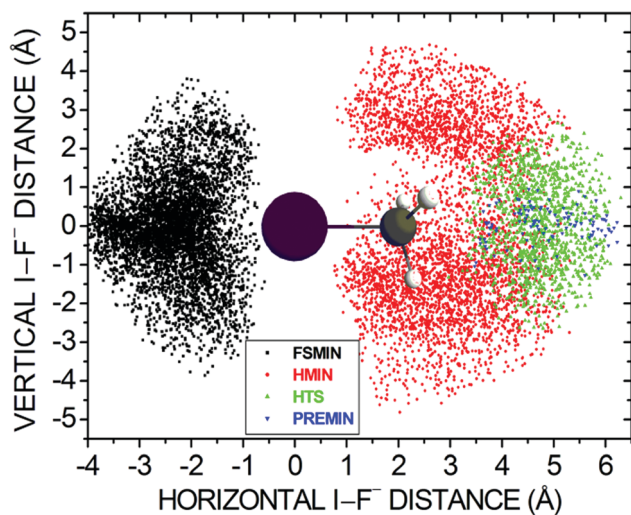


Fig. 3 Stationary-point-specific distributions of the positions of F^- in the entrance channel of the $F^- + CH_3I$ reaction obtained by trajectory orthogonal projection¹⁶ onto the I-C-H plane at a collision energy of $35.3 \text{ kcal mol}^{-1}$.

in agreement with our previous work.¹⁶ In the present work we can also distinguish between H-bonded and ion-dipole complexes in the back-side region, and as Fig. 3 and Fig. S2 (ESI[†]) show, PREMIN-like structures are localized in a much smaller configuration space than HMIN geometries, this is the reason why the overall probability of HMIN formation is significantly larger than that of the usual C_{3v} ion-dipole complex formation even if the probability density of F^- at the PREMIN stationary point is high. The above-described findings are similar at all the collision energies; just the distributions become broader as the collision energy increases (Fig. S2, ESI[†]). Besides the long time spent in the entrance-channel, complex formation in the exit channel (POSTMIN) is also significant for the S_N2 inversion and retention channels. POSTMIN formation is not expected for the induced-inversion and abstraction channels. Indeed, at low collision energies the POSTMIN probability is zero or negligible for the induced-inversion and abstraction pathways; however, at higher collision energies small POSTMIN probabilities are found for both channels (see Fig. S1, ESI[†]). Animations show that trajectories can cross the WALDENTS and after entering into the POSTMIN region recrossing may occur, which can be followed by proton abstraction leading to induced inversion or $HF + CH_2I^-$ products. Note that significant recrossing in identity S_N2 reactions, $Cl^- + CH_3Cl$ (ref. 27) and $F^- + CH_3F$ (ref. 28), was found earlier, here we show that recrossing can occur for a highly-exothermic system as well. Furthermore, at high collision energies an occasional $FH \cdots CH_2I^- \leftrightarrow (HF)-CH_2 \cdots I^-$ arrangement can result in assignments to POSTMIN with large RMS values. The WALDENTS probability is clearly the most significant for the S_N2 inversion channel, followed by S_N2 retention, because the latter also involves Walden inversion as the second step of the double-inversion process. However, the WALDENTS probability is usually only a few % for S_N2 inversion and even less for retention, revealing that the trajectories pass the saddle-point region fast.

As seen in Fig. 1, there are many stationary points involved in the abstraction channel and the role of them has been an open question. The present analysis shows that the trajectories visit most of the abstraction stationary points with significant probability. Somewhat surprisingly this is not just true for the proton-transfer reaction, but for all channels showing that the title reaction is indirect as previous studies proposed.²⁹ Nevertheless, the abstraction stationary points become more dominant for the abstraction channel as the collision energy increases and the reaction becomes more direct. The only stationary point which has negligible probability is TS2, where FH connects to the I atom of the ICH_2^- unit with nearly collinear $FH \cdots IC$ arrangement. The DITS is involved in the proton-transfer pathways, but usually with lower probability than the other abstraction stationary points. Furthermore, most of the abstraction stationary points play significant roles in the S_N2 retention mechanism, often with larger probability than DITS, showing that double inversion is an indirect process, where the HF unit is moving around CH_2I^- until eventually a DITS-like structure is formed, where the first inversion occurs fast without the system staying at the DITS region for a long time. Of course, S_N2 retention can proceed *via* the front-side attack mechanism, which makes the above discussion less unambiguous. Fortunately, the induced-inversion channel, which produces an inverted reactant *via* DITS, allows us to elucidate the role of the stationary points in the first step of the double inversion. Similar to the above findings for S_N2 retention, the abstraction stationary points are formed during the induced-inversion process. Trajectory configurations are assigned to FSTS with significant probability for all channels. For the S_N2 retention channel front-side attack mechanism is expected at high collision energies explaining the large FSTS probabilities in these cases. For the other cases FSTS may cover the configuration space between HMIN and POSTMIN, resulting in many geometries assigned to FSTS, but these structures may not overlap well with the FSTS stationary point, just the other stationary points are even further away. This will be investigated in more detail below.

C. Distance distributions

Now we address the question how close the trajectories approach the stationary points in the title reaction. In Fig. S3-S9 (ESI[†]) and in the representative Fig. 4, we show the distributions of the $RMS(k)$ values, eqn (4), for each reaction channel. The distributions are presented for all the assigned stationary points, where $RMS(k)$ is minimized with respect to the stationary points (k), and for all $RMS(k)$ values without assignment. It is important to notice that these $RMS(k)$ distributions do not have a maximum at the origin, but the distributions often peak around 0.5 \AA , or in some cases at larger values, for the assigned stationary points. This demonstrates that the trajectories do not go exactly through the stationary points. (Note that the vanishing probabilities at $RMS(k) = 0$ is expected as we convert multi-dimensional distributions into one-dimensional distance distributions from a point in the configuration space.) To understand the meaning of this 0.5 \AA deviation, we should realize that the present definition of $RMS(k)$ corresponds to the root-mean-square value of the $R(H_1-H_1')$,

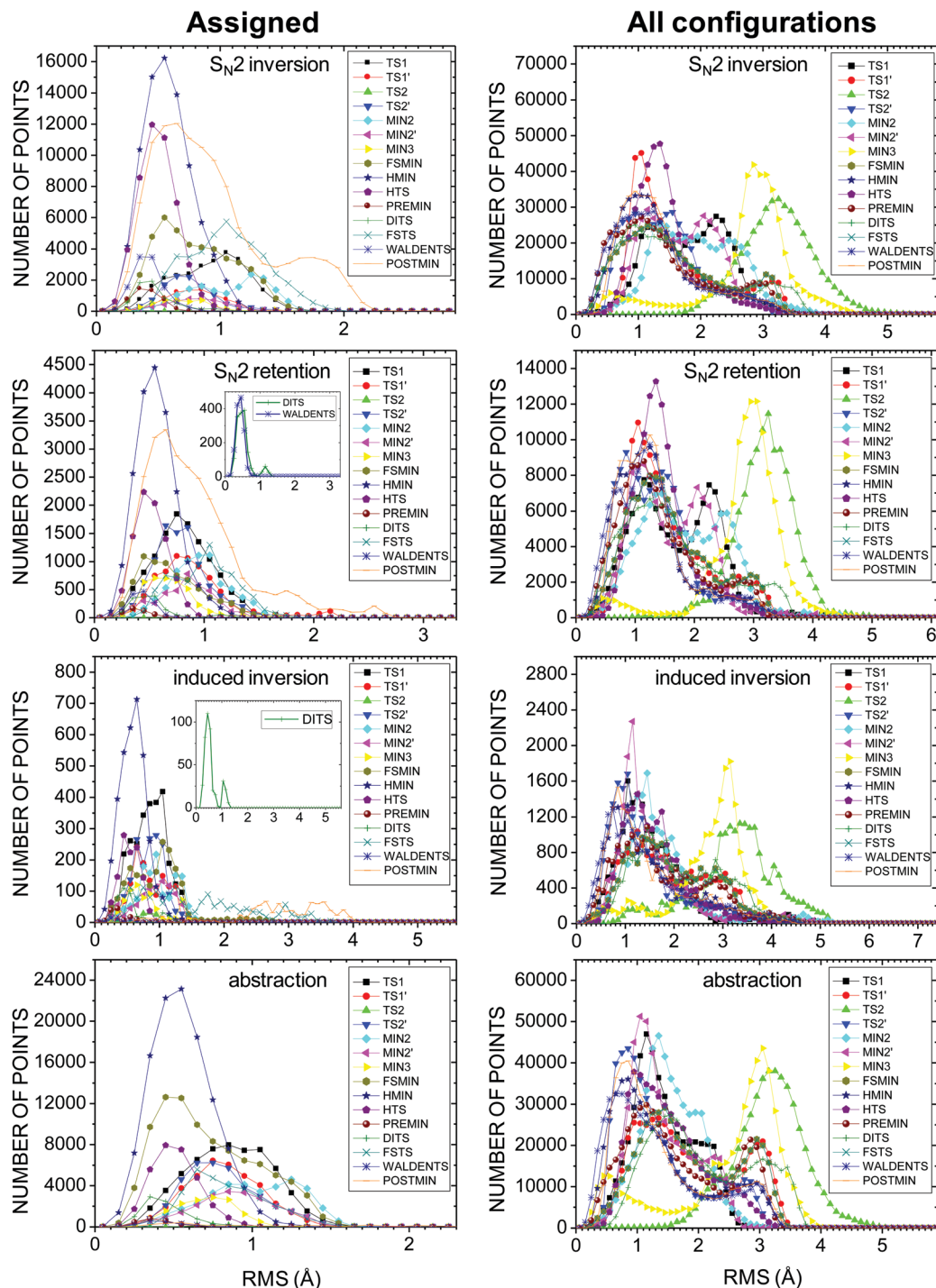


Fig. 4 Distributions of the root-mean-square deviations of the actual geometries relative to the assigned and all the stationary points of the $F^- + CH_3I$ reaction at $b = 0$ and collision energy of $35.3 \text{ kcal mol}^{-1}$.

$R(H_2-H_2')$, $R(H_3-H_3')$, $R(C-C')$, $R(F-F')$, and $R(I-I')$ distances, where $'$ labels the atoms of the stationary point. For FSMIN, HMIN, HTS, and PREMIN the assigned configurations are usually in the 0–1 Å RMS interval, most likely around 0.5 Å. For POSTMIN the distribution is broader, also has a maximum around 0.5 Å, but extends up to 1.5–2 Å. Of course, the long-range tails of the entrance- and exit-channel distributions depend on the definition

of the interaction region. As we mentioned above substantial number of configurations are assigned to FSTS, but their RMS distributions often peak around 1 Å and correspond to larger average distance deviations than those of FSMIN, HMIN, HTS, and PREMIN as well as WALDENTS, whose distribution also peaks around 0.5 Å. Considering the RMS distances of every geometry from all the stationary points, the $RMS(k)$ distributions

show that MIN3 and TS2 are usually the farthestmost stationary points with RMS values of 3–4 Å. Both MIN3 and TS2 correspond to $\text{FH}\cdots\text{ICH}_2^-$ structures as Fig. 1 shows, and these stationary points, especially TS2, are rarely assigned to a trajectory-geometry. Furthermore, all the assigned abstraction stationary points show distributions shifted toward larger RMS values than those of the $\text{S}_{\text{N}}2$ inversion stationary points. However, the DITS distributions are localized around RMS values of 0.5 Å (see Fig. 4), showing that even if the trajectories do not spend long time near this stationary point they pass this region in the vicinity of DITS.

D. Transition probabilities

To gain more insight into the dynamics of the title reaction we determine transition probability matrices ($P_{k,l}$) by counting $k \rightarrow l$ transitions between the k th and l th stationary points and setting $P_{k,l} = 0$ if $k = l$. The visual representation of the matrices at different collision energies are shown in Fig. S10–S16 (ESI[†]) and an example at collision energy of 35.3 kcal mol⁻¹ is shown in Fig. 5.

The matrices are almost symmetric, *i.e.*, $k \rightarrow l$ and $l \rightarrow k$ transitions have similar probabilities, showing that the $\text{F}^- + \text{CH}_3\text{I}$ reaction is indirect and the reaction pathways *via* consecutive stationary points are not dominant. From the reactant region the reactive trajectories enter into the HMIN, HTS, and, with smaller probability, FSMIN regions. PREMIN is mainly accessed from HTS and WALDENTS is approached from PREMIN or more likely directly from HTS. WALDENTS of the $\text{S}_{\text{N}}2$ trajectories is followed by POSTMIN, except in the case of the retention trajectories at the highest collision energy of 50 kcal mol⁻¹, where WALDENTS \rightarrow POSTMIN transition is negligible due to the reduced probability of double inversion. For the $\text{S}_{\text{N}}2$ channels the matrices show significant FSTS \leftrightarrow POSTMIN transitions, because FSTS covers some of the post-reaction configuration space when $\text{FCH}_3\cdots\text{I}^-$ is far from the C_{3v} collinear structure. The $\text{S}_{\text{N}}2$ product region, however, is almost exclusively accessed from POSTMIN. Direct FSTS \rightarrow PRODUCT transitions are only seen at collision energy of 50 kcal mol⁻¹ for the retention channel

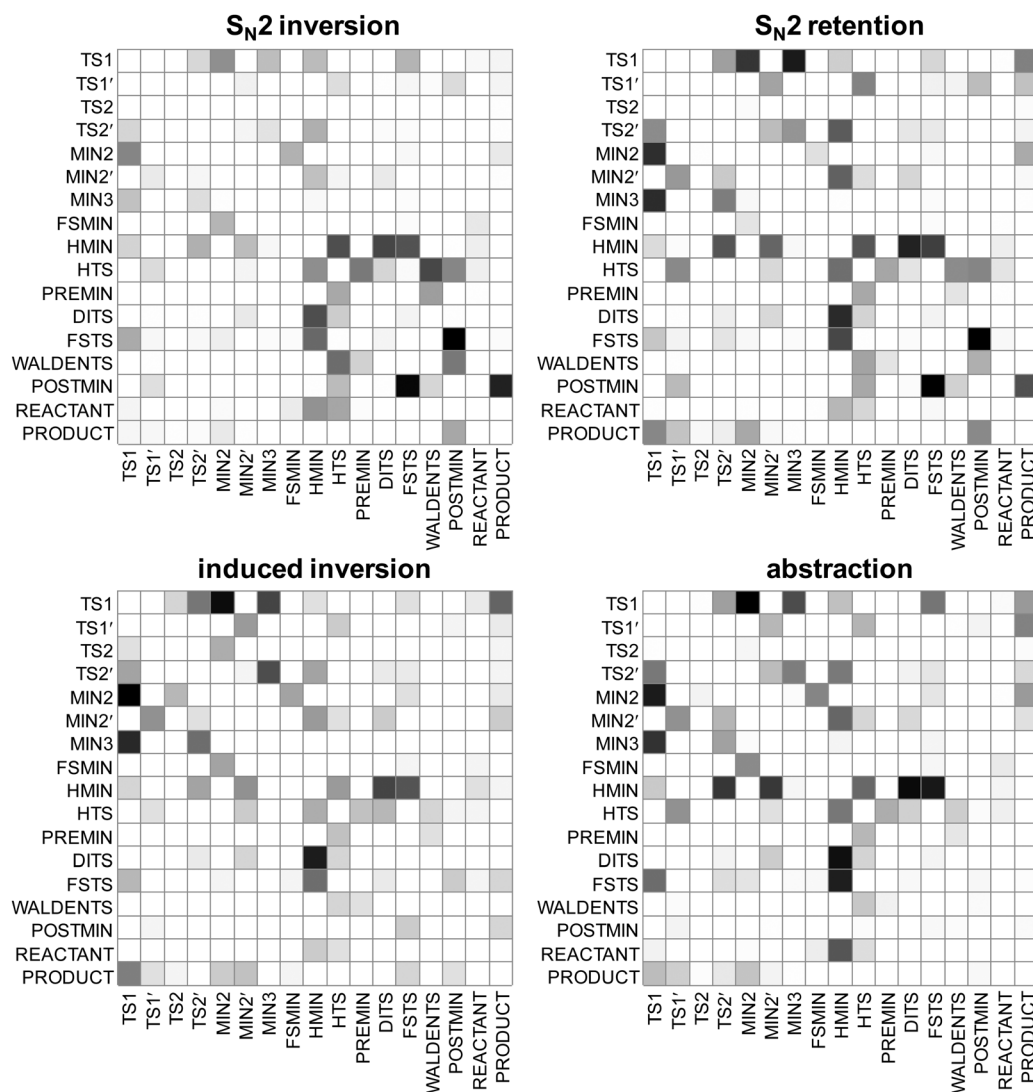


Fig. 5 Transition probability matrices for the stationary points of the $\text{F}^- + \text{CH}_3\text{I}$ reaction at $b = 0$ and collision energy of 35.3 kcal mol⁻¹. Darker matrix elements mean higher probabilities for row \rightarrow column transitions between stationary points.

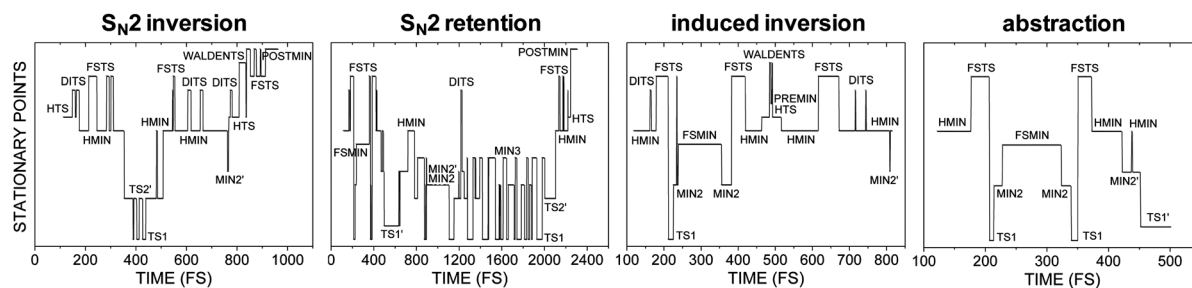


Fig. 6 Assigned stationary points as a function of integration time for selected trajectories of the $F^- + CH_3I$ reaction at $b = 0$ and collision energy of $35.3 \text{ kcal mol}^{-1}$. (The S_{N2} retention trajectory proceeds with double inversion.)

(Fig. S16, ESI[†]), indicating that front-side attack dominates retention at high collision energies. DITS is predominantly accessed from HMIN and trajectories most likely return to HMIN from DITS. For induced inversion and abstraction $MIN2 \leftrightarrow TS1$ transitions are the most dominant, see Fig. 1 for their similar structure. As Fig. 5 shows $TS2$ is almost never accessed as also seen in Fig. 2. The abstraction product region can be reached from $TS1$, $TS1'$, $TS2'$, $MIN2$, $MIN2'$, however, $MIN3 \rightarrow \text{PRODUCT}$ transitions are virtually not seen. This finding is interesting, because according to Fig. 1 and previous work,¹³ the proton-transfer pathways end *via* $MIN3$. Most of the above-discussed transitions can be observed in Fig. 6 and Fig. S17 (ESI[†]), where the assigned stationary points are shown as a function of time for selected trajectories. On the basis of the transition probability matrices and the time evolution of the stationary points we can conclude that the $F^- + CH_3I$ reaction dynamics and mechanisms are very complex even at high collision energies.

E. Distance and energy constraints

Thus far all the configurations in the interaction regions of the trajectories are assigned to stationary points even if in some cases the RMS distance is larger than 1 \AA as seen in Fig. 4 (left panels). Furthermore, as also shown in Fig. 4, the RMS distributions corresponding to various stationary points can be significantly different; therefore, the assigned structures do not cover the same size of configuration space for each stationary point. Thus, the results presented up to this point show the “catchment area” of different stationary points, thereby providing insights into the dynamics of a reactive system. One may apply various constraints during the assignment procedure, thereby restricting the configuration and/or energy space around the stationary points. In the present study we use distance constraints where a given structure is assigned to the closest stationary point (k) if the corresponding $RMS(k)$ value is less than a certain limit, for example, 0.5 , 1.0 , and 2.0 \AA , as shown in Fig. 7 and Fig. S18 (ESI[†]). We also show stationary-

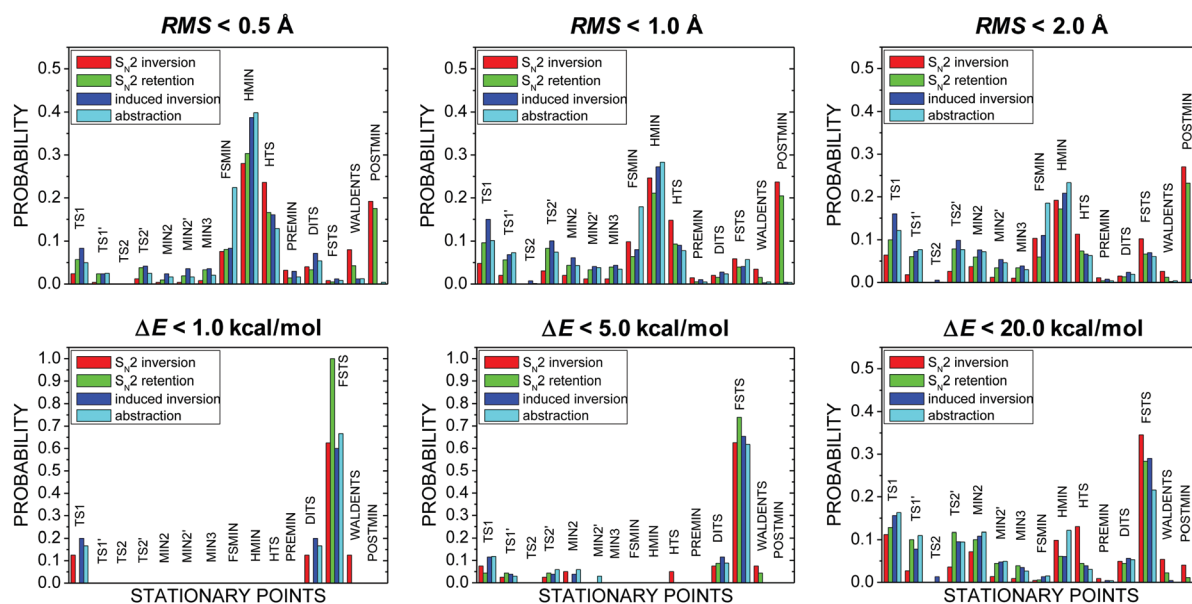


Fig. 7 Distance-constrained and energy-constrained stationary-point probability distributions, normalized for each channel, corresponding to $b = 0$ $F^- + CH_3I$ trajectories at a collision energy of $35.3 \text{ kcal mol}^{-1}$. Configurations are assigned to the closest stationary points if the RMS distance, eqn (4), is less than a given value (upper panels) or the absolute energy deviation, ΔE , between the potential energy of the actual geometry and that of the minimum-RMS stationary point is less than a given energy limit (lower panels).

point probability distributions in Fig. 7 and Fig. S19 (ESI[†]) with energy constraints assigning structures to stationary points based on the minimum RMS distance as before, but enforcing absolute energy difference between the given geometry and the assigned stationary point being less than, in the present case, 1.0, 5.0, and 20.0 kcal mol⁻¹. The distance-constrained distributions are similar with the 0.5, 1.0, and 2.0 Å limits, but notable subtle differences exist. FSTS and POSTMIN probabilities decrease as the stricter RMS constraints are applied, in accord with their broad RMS distributions shown in Fig. 4. At collision energy of 1.0 kcal mol⁻¹, the FSTS probability vanishes with a 0.5 Å constraint, as expected considering that FSTS is a high-energy stationary point. On one hand, the probabilities of WALDENTS and DITS as well as those of the pre-reaction stationary points, HMIN, HTS, and PREMIN, increase as the distance limit decreases, showing that the trajectories approach these stationary points closer than the others. On the other hand, the probabilities of the abstraction minima and transition states usually decrease as the distance constraint becomes stricter.

Considering the energy-constrained results, Fig. 7 and Fig. S19 (ESI[†]) show that FSTS probabilities usually increase with decreasing energy limit, except at the lowest collision energy of 1.0 kcal mol⁻¹, where the FSTS probability is zero, similar to the case of a strict distance constraint. POSTMIN probability decreases and DITS probability increases with energy constraints, in accord with the distance constraints. However, there are some seemingly surprising results, *i.e.*, POSTMIN probability becomes zero with 1.0 and 5.0 kcal mol⁻¹ energy limits and FSMIN, HMIN, HTS, and PREMIN probabilities are also zero or very small. The vanishing POSTMIN probability can be explained by the fact that POSTMIN is the global minimum of the potential energy surface where the CH₃F fragment is usually vibrationally highly excited, therefore, the potential energy of the FCH₃···I⁻ complex is often well above the minimum point. The very small pre-reaction stationary-point probabilities can be understood considering that CH₃I has a zero-point energy (ZPE) of 23.1 kcal mol⁻¹; therefore, in the entrance channel the zero-point vibration may increase the potential energy by a value fluctuating around 12 kcal mol⁻¹ (half of the ZPE). Thus, vibration decreases the chance for approaching the energy of the pre-reaction stationary points, whereas vibrational energy may help to reach the classical energy of higher-energy stationary points, like FSTS. One may consider applying the energy constraint using ZPE-corrected stationary-point energies, which may provide more realistic probabilities, though reactions do not necessarily follow the vibrationally adiabatic ground state potentials, for example, in the present case the CH₃F product is predominantly highly excited. In case one intends to apply ZPE corrections, consideration is warranted whether the ZPE or its half value (the mean potential energy of a harmonic oscillator is half of the total vibrational energy) should be added to the classical energy of the stationary points. On the basis of the present distance- and energy-constrained analyses, we conclude that the distance constraint is more promising than constraining the energy. Furthermore, we would like to emphasize that the non-constrained results also provide valid and useful insights into the dynamics of a chemical reaction, the various

constrained methods should be considered as complementary techniques providing results and additional insights from a different point of view.

IV. Summary and conclusions

We have described a stationary-point assignment technique, which can be implemented for any classical trajectory code, providing new insights into the mechanisms of chemical reactions, especially when many stationary points are involved and complex formation occurs in the dynamics. For the F⁻ + CH₃I reaction the analysis reveals non-traditional S_N2 dynamics with significant front-side and hydrogen-bonded back-side complex formation and small probabilities for ion-dipole pre-reaction complex. Most of the proton-transfer stationary points are involved in the double-inversion process, confirming the previous finding that double inversion is an indirect, non-IRC process.¹⁵ The trajectories go through the so-called double-inversion transition state fast, but approach the close vicinity of the stationary point indicating that this transition state plays an important controlling role of the double-inversion channel. Stationary-point transition probability matrices and time-evolution of the stationary points reveal the dominance of indirect mechanisms with several forward-backward transitions between the minima and transition states. Distance- and energy-constraints provide additional insights into the dynamics by restricting the configuration and/or energy space around the stationary points, whereas the non-constrained assignment uncovers the “catchment area” of different minima and transition states. Future studies could apply the present methodology for direct reactions, where the analysis may reveal pathways with consecutive stationary points without any recrossing.

Conflicts of interest

There are no conflicts of interest to declare.

Acknowledgements

We thank the National Research, Development and Innovation Office – NKFIH, K-125317 (G. C.), the Ministry of Human Capacities, Hungary grant 20391-3/2018/FEKUSTRAT (G. C.), and the Richter Scholarship (B. O.) for financial support. We acknowledge KIFÜ for awarding us access to resource based in Hungary at Szeged.

References

- 1 L. Sun, K. Song and W. L. Hase, *Science*, 2002, **296**, 875.
- 2 F. H. Stillinger and T. A. Weber, *Science*, 1984, **225**, 983.
- 3 G. Czakó and J. M. Bowman, *J. Chem. Phys.*, 2009, **131**, 244302.
- 4 G. Czakó, A. L. Kaledin and J. M. Bowman, *J. Chem. Phys.*, 2010, **132**, 164103.
- 5 G. Czakó, A. L. Kaledin and J. M. Bowman, *Chem. Phys. Lett.*, 2010, **500**, 217.

- 6 G. Czakó, *J. Phys. Chem. A*, 2012, **116**, 7467.
- 7 J. C. Corchado and J. Espinosa-Garcia, *Phys. Chem. Chem. Phys.*, 2009, **11**, 10157.
- 8 L. Ping, L. Tian, H. Song and M. Yang, *J. Phys. Chem. A*, 2018, **122**, 6997.
- 9 T. Tsutsumi, Y. Harabuchi, Y. Ono, S. Maeda and T. Taketsugu, *Phys. Chem. Chem. Phys.*, 2018, **20**, 1364.
- 10 J. Zhang, J. Mikosch, S. Trippel, R. Otto, M. Weidemüller, R. Wester and W. L. Hase, *J. Phys. Chem. Lett.*, 2010, **1**, 2747.
- 11 J. Mikosch, J. Zhang, S. Trippel, C. Eichhorn, R. Otto, R. Sun, W. A. de Jong, M. Weidemüller, W. L. Hase and R. Wester, *J. Am. Chem. Soc.*, 2013, **135**, 4250.
- 12 R. Sun, C. J. Davda, J. Zhang and W. L. Hase, *Phys. Chem. Chem. Phys.*, 2015, **17**, 2589.
- 13 J. Zhang, J. Xie and W. L. Hase, *J. Phys. Chem. A*, 2015, **119**, 12517.
- 14 B. Olasz, I. Szabó and G. Czakó, *Chem. Sci.*, 2017, **8**, 3164.
- 15 Y.-T. Ma, X. Ma, A. Li, H. Guo, L. Yang, J. Zhang and W. L. Hase, *Phys. Chem. Chem. Phys.*, 2017, **19**, 20127.
- 16 I. Szabó, B. Olasz and G. Czakó, *J. Phys. Chem. Lett.*, 2017, **8**, 2917.
- 17 T. Györi, B. Olasz, G. Paragi and G. Czakó, *J. Phys. Chem. A*, 2018, **122**, 3353.
- 18 P. Liu, J. Zhang and D. Y. Wang, *Phys. Chem. Chem. Phys.*, 2017, **19**, 14358.
- 19 X. Ma, X. Tan and W. L. Hase, *Int. J. Mass Spectrom.*, 2018, **429**, 127.
- 20 M. Stei, E. Carrascosa, A. Dörfler, J. Meyer, B. Olasz, G. Czakó, A. Li, H. Guo and R. Wester, *Sci. Adv.*, 2018, **4**, eaas9544.
- 21 A. Y. Dymarsky and K. N. Kudin, *J. Chem. Phys.*, 2005, **122**, 124103.
- 22 K. N. Kudin and A. Y. Dymarsky, *J. Chem. Phys.*, 2005, **122**, 224105.
- 23 G. Czakó and J. M. Bowman, *J. Phys. Chem. A*, 2014, **118**, 2839.
- 24 I. Szabó and G. Czakó, *J. Phys. Chem. A*, 2017, **121**, 9005.
- 25 I. Szabó and G. Czakó, *Nat. Commun.*, 2015, **6**, 5972.
- 26 W. Kabsch, *Acta Crystallogr., Sect. A: Cryst. Phys., Diffr., Theor. Gen. Crystallogr.*, 1976, **32**, 922.
- 27 Y. J. Cho, S. R. Vande Linde, L. Zhu and W. L. Hase, *J. Chem. Phys.*, 1992, **96**, 8275.
- 28 I. Szabó, H. Telekes and G. Czakó, *J. Chem. Phys.*, 2015, **142**, 244301.
- 29 M. Stei, E. Carrascosa, M. A. Kainz, A. H. Kelkar, J. Meyer, I. Szabó, G. Czakó and R. Wester, *Nat. Chem.*, 2016, **8**, 151.